

Influence of AlN barrier thickness on AlN/GaN heterostructure optical and transport properties

JIANFEI LI^{a,b}, YUANJIE LV^b, SHULAI HUANG^c, ZIWU JI^{a,*}, ZHIYONG PANG^a, XIANGANG XU^d

^a*School of Microelectronics, Shandong University, Jinan 250100, China*

^b*Science and Technology on Application-Specific Integrated Circuit (ASIC) Laboratory, Hebei Semiconductor Research Institute, Shijiazhuang 050051, China*

^c*Science and Information College, Qingdao Agricultural University, Qingdao 266109, China*

^d*Key Laboratory of Functional Crystal Materials and Device (Ministry of Education), Shandong University, Jinan 250100, China*

AlN/GaN heterostructures, with different AlN barrier thicknesses (3 and 6 nm), are characterized using atomic force microscopy, high-resolution transmission electron microscopy, photoluminescence, and Hall effect measurements. Based on the measured results, we suggest that with increased AlN barrier thickness, the tensile strain in the AlN barrier layer is relaxed by crack channels. In addition, the strain-induced cracking also greatly penetrated into the GaN buffer layer, and resulted in the relaxation of the compressive strain and the increase of the defects in the GaN buffer layer. This caused AlN/GaN heterostructure quality deterioration and introduced additional scattering.

(Received September 23, 2015; accepted April 6, 2017)

Keywords: Strain relaxation, Hall effect, Photoluminescence, Crack

1. Introduction

High electron mobility transistors (HEMTs) based on AlGaIn/GaN heterostructures, which contain a polarization-induced high-mobility two-dimensional electron gas (2DEG) at the AlGaIn/GaN interfaces even in the absence of any doping, have been widely studied for their potential application in high-frequency and high-power amplifiers [1–3]. Recently, high-quality AlN/GaN heterostructures with thin AlN barriers, compared with the AlGaIn/GaN heterostructures, have had improved device performance due to the increased quantum confinement and 2DEG density originating from the large conduction band offset between AlN and GaN and from the increased polarization-induced electric field in the AlN barrier layer. In addition, the reduced alloy scattering because of the all-binary AlN/GaN heterostructures also improved device performance [4–6]. Therefore, the expected reduction in gate leakage current, short channel effects, and current collapse makes the AlN/GaN structure a strong candidate for high-frequency and high-power applications [7,8]. The high quality of AlN/GaN HEMTs typically implies the combination of a large electron sheet density and high mobility. It has been reported that the transport properties of these structures depend strongly on the AlN barrier thickness [5,6,8–10]. On one hand, increased AlN barrier thickness provides a high density of carriers and good confinement of the 2DEG, as mentioned above. On the other hand, the increased AlN barrier thickness also

simultaneously results in an increased effective total strain energy present in the system. When the AlN barrier thickness increased beyond a critical value, the tensile strain-induced cracking in the AlN barrier layer occurred. Consequently this may lead to transport property deterioration in the AlN/GaN structure. Although the reports showed the atomic force microscopy (AFM) images of the AlN surfaces to evidence the relaxation of the tensile strain in the AlN barrier layer by cracking, further information on the mechanism of the cracks propagating downward from the AlN barrier layer and the effect of the cracks on the GaN quality was not given. Therefore, a further investigation of the influence of the AlN barrier thickness on the structural quality of the AlN/GaN heterostructure is deemed necessary to improve the transport properties of these structures. However, due to the lattice mismatch problem (2.4% for AlN on GaN), much less work has been done on the AlN/GaN structure for HEMT devices mainly due to the difficulty of growing high-quality AlN barrier layers on GaN [6,11,12].

In this study, to understand the origin and propagation mechanism of the cracks and the effect of the cracks on the AlN/GaN heterostructure quality, the influence of the AlN barrier thickness on the optical and transport properties of an AlN/GaN heterostructure was investigated by atomic force microscopy (AFM), high-resolution transmission electron microscopy (HRTEM), photoluminescence (PL), and Hall effect measurements. It is suggested that, with increased AlN barrier thickness, the

strain-induced cracking results in a relaxation of the tensile (compressive) strain in the AlN barrier (GaN buffer) layer, and increased structural and point defects in both layers. This causes a deterioration in the quality of the AlN/GaN heterostructure, and introduces additional scattering.

2. Experiment

The AlN/GaN heterostructures used in this study were epitaxially grown by metal-organic chemical vapor deposition (MOCVD) on (0001) sapphire substrates. Each AlN/GaN heterostructure consisted of a 100-nm-thick low-temperature AlN nucleation layer, followed by a 2- μm -thick unintentionally doped GaN buffer layer, an AlN barrier layer, and a 2-nm-thick GaN cap. The AlN barrier thickness was 3 nm for sample A and 6 nm for sample B.

The surface morphologies and material qualities of the samples were assessed by AFM and HRTEM, respectively. For PL measurements, the samples were mounted in a closed-cycle He cryostat and the temperature was held at 6 K. The 325 nm line of a He-Cd laser was used as an excitation light source with a spot size of approximately 250 μm . The PL signal from the sample was dispersed by a Jobin-Yvon iHR320 monochromator and detected by a thermoelectrically cooled Synapse CCD detector. In addition, Hall effect measurements were performed in Van der Pauw geometry on 10 mm square sample at room temperature. Indium was used to form the Ohmic contacts to the structures under investigation.

3. Results and discussions

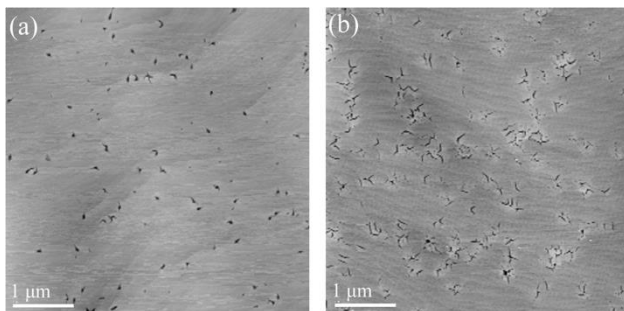


Fig. 1. AFM images of the surface morphologies of samples A (a) and B (b)

Typical AFM images of the surface morphologies of samples A and B are shown in Fig. 1. The AFM images for samples A and B display a stepped/terraced structure with a mean roughness of 0.357 and 0.366 nm over a 5 μm square, respectively. Moreover, the surface of sample A is filled by a mix of pit-like and micro-crack structures with a density of about $3.5 \times 10^8 \text{ cm}^{-2}$, as shown in Fig. 1(a). In contrast, surface pits were almost invisible, but higher density (about $9.8 \times 10^8 \text{ cm}^{-2}$) of cracks with longer crack

lines are observed in sample B (Fig. 1(b)). The pits are generally thought to be the surface termination of threading dislocations or the flaws in the material, and can act as nucleation sites for cracks [13–15], while the cracks are attributed to the relaxation of the tensile strain in the AlN barrier layer [5]. To further investigate the origin of the pits and cracks, typical cross-sectional HRTEM images of these two samples are shown in Fig. 2. For sample A, in addition to a few threading dislocations that penetrated the GaN buffer layer and AlN barrier layer along the c-axis from the low-temperature AlN nucleation layer and reached the AlN surface where pits or cracks are formed [16,17], more cracks that penetrated into the GaN buffer layer from the AlN barrier layer are observed [11,13], as shown in Fig. 2(a) and (c). In contrast, sample B showed a higher density of cracks with greater penetration depths in the GaN buffer layer (see Fig. 2(b) and (d)). The evolution trend of the cracks with increasing AlN barrier thickness observed in Fig. 2 is consistent with that observed in Fig. 1. All of the characteristics shown in Figs. 1 and 2 indicate that the majority of the observed cracks propagated downward from the AlN barrier layer, rather than upward from the film/substrate interface. Therefore it is suggested that, in the present study, with increased AlN barrier thickness the tensile strain in the AlN barrier layer can be relaxed by crack channels, and the strain-induced cracking also greatly penetrated into the GaN buffer layer and resulted in compressive strain relaxation in the GaN layer.

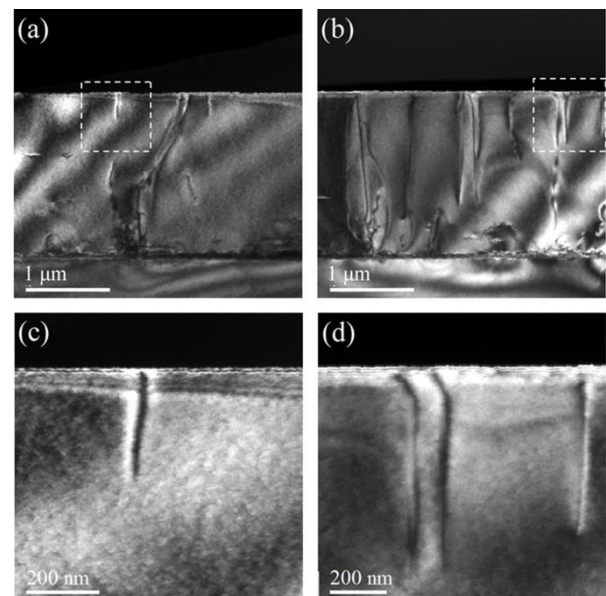


Fig. 2. Cross-sectional TEM image of samples A (a) and B (b). (c) and (d) display the enlarged view of the squared regions in (a) and (b), respectively

The PL spectra of these two samples measured at 6 μW and 6 K are shown in Fig. 3. The PL spectra for both

samples show three main transitions from the GaN epitaxial layer [18,19]. Namely, a near-band edge (NBE) emission centered at approximately 3.485 eV, which originated from the flat-band region of the GaN layer; a well-known ultraviolet luminescence (UVL) band at approximately 3.290 eV, which is considered to be related to the transition between the conduction-band or shallow-donors and the shallow-acceptors; and a very weak broad yellow luminescence (YL) band at approximately 2.2 eV ascribed to the transition between the conduction-band or shallow-donors and deep acceptors. The intensity oscillations of the YL emission are due to Fabry–Perot type interferences [20]. In addition to these main transitions, phonon replicas of the NBE and UVL peaks, denoted by NBE-LO and UVL-LO, can be seen in Fig. 3. The LO phonon energy in GaN was about 91 meV [18,19]. Moreover, it is also noted from Fig. 3 that the position of the NBE peak in the PL spectra for samples A and B is shifted by approximately 16 and 12 meV towards higher energies in comparison with that of strain-free GaN layers, respectively [18,21]. This can be explained by the thermal mismatched expansion coefficient between the GaN buffer layer and the sapphire substrate. There is a compressive strain in the GaN buffer layer which resulted in a blue-shift of the NBE peak for both samples relative to the strain-free GaN layers.

Furthermore, by comparing the PL spectra of these two samples shown in Fig. 3, it is found that the PL spectrum is dominated by a strong NBE emission for sample A (Fig. 3(a)), but by a strong UVL emission with more phonon replicas, up to UVL-3LO, for sample B (Fig. 3(b)). Also, the NBE peak of sample B exhibited a slight red-shift of approximately 4 meV relative to that of sample A. That is, in contrast to sample A, sample B showed a weaker NBE emission accompanied by the red-shift of its peak and a stronger defect-related UVL emission. The results can be explained by the strain-induced cracking effect produced by the tensile (compressive) strain relaxation in the AlN barrier (GaN buffer) layer from the increased AlN barrier thickness, from 3 to 6 nm, and the increased structural and point defects in the GaN buffer layer [5,9–11]. However, in contrast, no obvious change is observed in the YL band in the PL spectra when the AlN barrier thickness is increased. This may be because the YL band is mainly related to native defects and residual impurities caused during the growth of the GaN buffer layer, and most of the native defects and residual impurities exist in the interface region between the GaN buffer layer and the low-temperature AlN nucleation layer [22].

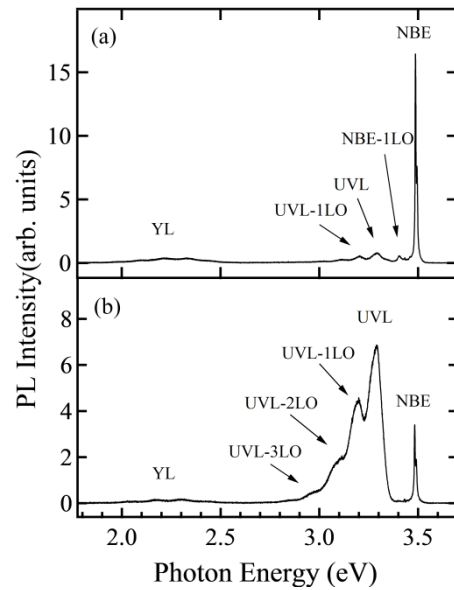


Fig. 3. PL spectra of samples A (a) and B (b) measured at 6 μ W and 6 K

Moreover, to investigate the influence of AlN barrier thickness on the conduction mechanism, the sheet carrier density and Hall mobility of both samples, as a function of temperature from 10 K to room-temperature, were measured. As shown in Fig. 4, the measured sheet electron densities for both samples A and B are nearly temperature-independent constants of about 1.9×10^{13} and 3.0×10^{13} cm^{-2} , respectively. This indicates an absence of any significant parallel conduction paths in both samples [10]. The high values of the sheet electron densities for both samples were caused by spontaneous and piezoelectric polarization fields in the AlN barrier layers [9,10,23]. In contrast, the electron mobilities for both samples were nearly temperature-independent constants below approximately 90 K, and then showed a significant decrease with further increased temperature: this is due to the dominance of optical phonon scattering at higher temperatures [5,8,23,24]. The measured electron mobilities for samples A and B are 7324 and 1521 cm^2/V at 10 K, and 1068 and 390 cm^2/V at room-temperature, respectively. All of these Hall measurement results show that, in the present study, two nominal AlN/GaN 2DEG structures have been successfully grown on sapphire substrates [9].

In addition, by comparing the Hall measurement results, increasing the AlN barrier thickness from 3 to 6 nm also increased the density of the 2DEG, and decreased the mobility of the 2DEG, over the whole temperature range. This behavior indicates that both the density and mobility of the 2DEG are affected by a small change in AlN barrier thickness. The increased electron density with increased AlN barrier thickness can be explained as follows: the surface donor states residing at the top of the AlN surface are the primary source of the 2DEG electrons

present at the AlN/GaN interface [3,24,25]. With increased AlN barrier thickness, the surface donor energy level will increase toward the Fermi level due to the existence of the polarization field in the AlN barrier layer. Once it reaches the Fermi level, the surface donor states are ionized, and start donating electrons to form the 2DEG at the AlN/GaN interface [3,24]. Therefore, sample B has a higher density of 2DEG electrons than sample A due to its thicker barrier [5,6,8,10]. On the other hand, the electron mobility drastically decreased with increased AlN barrier thickness. It cannot be expected that this will be explicable by either the scattering from the remote ionized impurities that might be present in the AlN barrier, or by the scattering from the residual impurities in the GaN channel, because increased AlN barrier thickness increased the 2DEG density, which can improve the screening of impurities in both cases [24]. This behavior also cannot be attributed to an alloy disorder scattering due to the all-binary AlN/GaN heterostructure [4–6]. In contrast, the interface roughness scattering is expected to increase. The increased interface roughness scattering with increasing AlN barrier thickness from 3 to 6 nm, can be mainly attributed to the following two factors: 1) the 2DEG electrons are pushed closer to the interface at higher 2DEG electron densities [5,9]; 2) deterioration of AlN/GaN interface quality due to the increased surface roughness and to the cracking effect enhancement [5,9,10], as shown in Figs. 1 and 2.

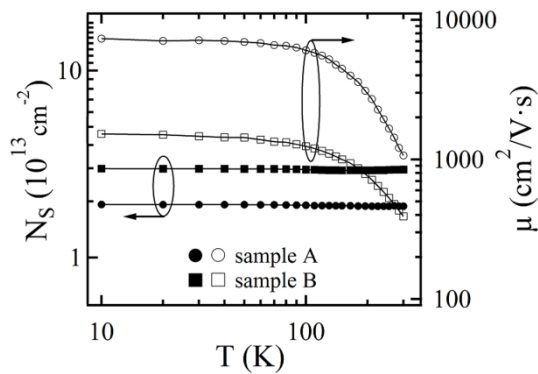


Fig. 4. Temperature dependences of the sheet carrier density and Hall mobility in the samples A (circles) and B (squares)

With the Hall measurement results, the calculated square resistances for samples A and B are 44 and 138 Ω/\square at 10 K, and 311 and 542 Ω/\square at room-temperature, respectively. That is, as the AlN barrier thickness increased from 3 to 6 nm, although the sheet electron density increased, the sheet resistance increased both at 10 K and at room-temperature due to the decreased electron mobility. It has been reported that a critical AlN barrier thickness around 3.7 nm is observed in similar AlN/GaN heterostructures [5,8,9]. As described in these reports, with increased AlN barrier thickness, the sheet resistance decreased below the critical thickness due to the increased or almost constant electron mobility in the barrier

thickness range. It then increased with further increased AlN barrier thickness because of the decreased electron mobility originating from the marked cracking effect enhancement. Together with the reported results, we can infer that the 6 nm-thick AlN barrier should be above critical thickness since sample B showed a marked increase in the sheet resistance compared with sample A, as shown in Fig. 3. However, to obtain some of the key parameters, such as the critical thickness, maximum mobility and minimum resistance, more careful experimental investigation are required to show a clear trend in defect density and GaN quality, and these remain to be done in our future work. The experimental results obtained in the present work, are expected to provide useful guidance to scientists involved in the fabrication of high-performance AlN/GaN HEMTs.

4. Conclusions

In conclusion, the AlN barrier thickness's influence on the surface morphologies, material qualities, and optical and transport properties, of an AlN/GaN heterostructure was investigated by AFM, HRTEM, PL and Hall measurements. The measurement results showed that compared with the sample with a thin AlN barrier (3 nm), the sample with a thicker barrier (6 nm) had a higher density of cracks with greater penetration depths, and showed defect-related UVL emission enhancement, weakened NBE emission accompanied by its peak red-shift, and significantly decreased electron mobility. The results can be explained by the fact that, with increased AlN barrier thickness, the strain-induced cracking effect resulted in strain relaxation and increased AlN/GaN heterostructure defects. This caused a deterioration in heterostructure quality, and introduced additional scattering. To obtain high-quality AlN/GaN HEMTs, further experimental and theoretical investigation is required for a complete understanding of the structural, optical and transport properties of the AlN/GaN heterostructure.

Acknowledgements

This work was supported by the Key Laboratory of Functional Crystal Materials and Device (Shandong University, Ministry of Education) (Grant No. JG1401), the Postdoctoral Science Foundation of China (No. 2016T90782), the National Natural Science Foundation of China (Grant Nos. 51672163 and 61306113), and the Major Research Plan of the National Natural Science Foundation of China (Grant No. 91433112).

References

- [1] X. Y. Liao, K. Zhang, C. Zeng, X. F. Zheng, Y. F. En,

- P. Lai, Y. Hao, *Chin. Phys. B* **23**, 057301 (2014).
- [2] X. G. He, D. G. Zhao, D. S. Jiang, *Chin. Phys. B* **24**, 067301 (2015).
- [3] N. Goyal, T. A. Fjeldly, *J. Appl. Phys.* **113**, 014505 (2013).
- [4] J. T. Zhao, Z. J. Lin, C. B. Luan, Y. J. Lv, Z. H. Feng, M. Yang, *Chin. Phys. B* **23**, 127104 (2014).
- [5] Y. Cao, D. Jena, *Appl. Phys. Lett.* **90**(18), 182112 (2007).
- [6] A. M. Dabiran, A. M. Wowchak, A. Osinsky, J. Xie, B. Hertog, B. Cui, D. C. Look, P. P. Chow, *Appl. Phys. Lett.* **93**(8), 082111 (2008).
- [7] Y. J. Lv, Z. H. Feng, Z. J. Lin, G. D. Gu, S. B. Dun, J. Y. Yin, T. T. Han, S. J. Cai, *Chin. Phys. B* **23**, 027101 (2014).
- [8] D. A. Deen, D. F. Storm, D. J. Meyer, R. Bass, S. C. Binari, T. Gougousi, K. R. Evans, *Appl. Phys. Lett.* **105**(9), 093503 (2014).
- [9] I. P. Smorchkova, S. Keller, S. Heikman, C. R. Elsass, B. Heying, P. Fini, J. S. Speck, U. K. Mishra, *Appl. Phys. Lett.* **77**(24), 3998 (2000).
- [10] I. P. Smorchkova, L. Chen, T. Mates, L. Shen, S. Heikman, B. Moran, S. Keller, S. P. DenBaars, J. S. Speck, U. K. Mishra, *J. Appl. Phys.* **90**(10), 5196 (2001).
- [11] V. V. Ursaki, I. M. Tiginyanu, V. V. Zalamai, S. M. Hubbard, D. Pavlidis, *J. Appl. Phys.* **94**(8), 4813 (2003).
- [12] K. Yagi, M. Kaga, K. Yamashita, K. Takeda, M. Iwaya, T. Takeuchi, S. Kamiyama, H. Amano, I. Akasaki, *Jpn. J. Appl. Phys.* **51**(5R), 051001 (2012).
- [13] S. Einfeldt, V. Kirchner, H. Heinke, M. Diebelberg, S. Figge, K. Vogeler, D. Hommel, *J. Appl. Phys.* **88**(12), 7029 (2000).
- [14] S. Einfeldt, H. Heinke, V. Kirchner, D. Hommel, *J. Appl. Phys.* **89**(4), 2160 (2001).
- [15] J. K. Sheu, M. L. Lee, W. C. Lai, *Appl. Phys. Lett.* **86**(5), 052103 (2005).
- [16] T. Kozawa, T. Kachi, H. Kano, H. Nagase, N. Koide, K. Manabe, *J. Appl. Phys.* **77**(9), 4389 (1995).
- [17] K. Hiramatsu, T. Detchprohm, I. Akasaki, *Jpn. J. Appl. Phys.* **32**(4), 1528 (1993).
- [18] J. P. Bergman, T. Lundström, B. Monemar, H. Amano, I. Akasaki, *Appl. Phys. Lett.* **69**(23), 3456 (1996).
- [19] M. A. Reshchikov, H. Morkoç, *J. Appl. Phys.* **97**(6), 061301 (2005).
- [20] T. Y. Lin, H. C. Yang, Y. F. Chen, *J. Appl. Phys.* **87**(7), 3404 (2000).
- [21] S. Dassonneville, A. Amokrane, B. Sieber, J. L. Farvacque, B. Beaumont, P. Gibart, *J. Appl. Phys.* **89**(7), 3736 (2001).
- [22] H. C. Yang, T. Y. Lin, Y. F. Chen, *Phys. Rev. B* **62**(19), 12593 (2000).
- [23] O. Ambacher, J. Smart, J. R. Shealy, N. G. Weimann, K. Chu, M. Murphy, W. J. Schaff, L. F. Eastman, R. Dimitrov, L. Wittmer, M. Stutzmann, W. Rieger, J. Hilsenbeck, *J. Appl. Phys.* **85**(6), 3222 (1999).
- [24] I. P. Smorchkova, C. R. Elsass, J. P. Ibbetson, R. Vetury, B. Heying, P. Fini, E. Haus, S. P. DenBaars, J. S. Speck, U. K. Mishra, *J. Appl. Phys.* **86**(8), 4520 (1999).
- [25] N. Goyal, T. A. Fjeldly, *Appl. Phys. Lett.* **105**(3), 033511 (2014).

*Corresponding author: jiziwu@sdu.edu.cn